



TECHNICAL ARTICLE

Microstructure Evolution and Hardness of Hypereutectic High Chromium Cast Iron after Tempering

Liu Yawei, Liu Wei, Yang Penghui, Fu Hanguang, Yin Wenhong, Jin Tounan, and Chen Zhengyang

Submitted: 28 November 2022 / Revised: 20 March 2023 / Accepted: 2 April 2023 / Published online: 20 April 2023

The effect of the tempering process on the microstructure evolution and hardness of 35 wt.%Cr-4 wt.%C Hypereutectic High Chromium Cast Iron (HHCCI) was studied by means of the scanning electron microscope and transmission electron microscope. The results show that with the increase in tempering temperature, the primary and eutectic carbides of HHCCI have no significant change, and the precipitation of secondary carbides in the matrix increases at first and then decreases. From the TEM analysis results, the secondary carbides after tempering are $M_{23}C_6$, which are rectangular, and with the extension of tempering time, a small part of eutectic carbides decompose and dissolve into the matrix, and the secondary carbides continue to precipitate and grow, and the length can reach several microns to more than 10 microns. With the increase in tempering temperature, the hardness of HHCCI increases, and the hardness tends to decrease when it exceeds 500 °C. After tempering for 6 h, the precipitation of secondary carbides in the matrix reaches the maximum, and the hardness of HHCCI reaches the maximum. After tempering holding time for more than 6 h, the hardness of HHCCI decreases continuously due to the aggregation and growth of secondary carbides.

Keywords hardness, holding time, hypereutectic high chromium cast iron, microstructure evolution, tempering temperature

1. Introduction

High chromium white cast iron is the third generation of wear resistant cast iron developed on the basis of common white cast iron and nickel hard white cast iron. In its microstructure, the triangular system M_7C_3 carbides with hardness greater than 1800 HV are fixed on the martensite or austenite matrix, and this material has high hardness and excellent wear resistance (Ref 1, 2). At present, High Chromium Cast Iron (HCCI) is widely used in metallurgy, mining, electric power, building materials, and other industries. Its popularization and application have remarkable economic and social benefits. In order to further improve the wear resistance of HCCI, it is an important trend to develop Hypereutectic High Chromium Cast Iron (HHCCI) by increasing the content of Cr and C and increasing the number of

primary carbides. As-cast HHCCI is mainly composed of austenitic matrix, eutectic and primary M_7C_3 carbides (Ref 3), and the content of carbides in HHCCI is generally higher than 40%. More M_7C_3 carbides give the material higher hardness and excellent wear resistance. However, higher C content will make the material brittle and reduce toughness (Ref 4). In order to adjust the morphology, size, quantity, and distribution of the microstructure, heat treatment of the material is required to obtain better hardness and wear resistance (Ref 5-7).

The common heat treatment methods are quenching and tempering (Ref 8). The matrix microstructure of as-cast HHCCI is mainly austenite with low hardness (Ref 9). The transformation of austenite to martensite and the simultaneous precipitation of fine secondary carbides can be achieved by appropriate heat treatment, which is important for improving the mechanical properties of HHCCI (Ref 10). Zhou et al. (Ref 11) investigated the effect of tempering temperatures at 200, 400, and 500 °C on 26 wt.%Cr HCCI and found that eutectic carbides would dissolve and lead to the size reduction with the increase in temperature. The hardness reaches a local maximum, and then decreases. Inthidech et al. (Ref 12) found that the hardness decreased and then increased with a successive number of tempering cycles. The volume fraction of retained austenite decreased gradually with increasing temperature and repeated tempering. Alejandro et al. (Ref 13) found that 3 wt.%C-25 wt.%Cr HCCI would obtain the best wear resistance after quenching at 1050 °C for 5 h and tempering at 400 °C for 2 h. Farah et al. (Ref 14) found that high chromium cast iron could obtain the best wear resistance and toughness after tempering at 450 °C and holding for 6 h, which was attributed to the effective dissolution of carbides and a small amount of retained austenite. Singh et al. (Ref 15) investigated different tempering temperatures and found that tempering at 500 °C could obtain the best combination of hardness, abrasion resistance, and impact toughness, and the tempering tempera-

Liu Yawei, Liu Wei, Fu Hanguang, Jin Tounan, and Chen Zhengyang, Key Laboratory of Advanced Functional Materials, Ministry of Education, School of Materials Science and Engineering, Research Institute of Advanced Materials Processing Technology, Beijing University of Technology, Amount 100, Pingle Garden, Chaoyang District, Beijing 100124, People's Republic of China; Yang Penghui, School of Materials Science and Engineering, Lanzhou University of Technology, Lanzhou 730050 Gansu Province, People's Republic of China; Yin Wenhong, Gangnuo New Materials Co., Ltd., Handan 057650 Hebei Province, People's Republic of China. Contact e-mail: hgfu@bjut.edu.cn.

tures above 500 °C would result in an increase in impact toughness and a decrease in hardness and wear resistance. However, a large amount of heat treatment studies focused on the field of hypoeutectic high chromium cast iron, and few studies focused on the heat treatment of HHCCI. In order to improve the comprehensive properties of HHCCI, an in-depth research is urgently needed on the heat treatment of HHCCI, especially the tempering heat treatment. The research group studied the effect of quenching heat treatment on the microstructure and properties of HHCCI in the early stage, and found that after quenching at 1000-1050 °C, it has high hardness and good wear resistance (Ref 16). Based on the previous research, the author designed the tempering temperature and tempering holding time of different process parameters to explore the effects of temperature and holding time on the tempering microstructure evolution and hardness of HHCCI, looking forward to providing a reference for the formulation of HHCCI tempering process.

2. Experimental

2.1 Sample Preparation and Heat Treatment

Hypereutectic high chromium cast iron was smelted in a 15 kg medium frequency induction furnace. Part of high-carbon ferrochromium and scrap steel was first placed at the bottom of the electric furnace, then ferromolybdenum and ferromanganese were added to mix and heat to melt, and the remaining ferrochromium was added after melting. The molten iron was heated to 1550 °C, 0.12 wt.% Al was added as a deoxidizer, and the molten iron was poured into the ladle immediately after deoxidization. 0.6 wt.% rare earth magnesium alloy modifier was pre-added to the ladle, and the composition of the modifier was 5 Mg, 2 RE, 40 Si, 2 Ca (wt.%). When the molten iron temperature dropped to 1465 °C, it was cast into a 120 × 150 × 25 mm square test block; the chemical composition of the material was determined by XRF, as shown in Table 1.

Combined with the previous research results of the research group (Ref 16), the quenching process was designed to heat the sample to 1025 °C for 1 h and then air cooling to room temperature. After quenching, the sample was tempered to eliminate the internal stress generated during quenching. Different process parameters of tempering temperature and tempering holding time were designed. The tempering temperature was set at 200, 400, 500, and 600 °C for 3 h, furnace-cooled. The samples were recorded as QT200, QT400, QT500, and QT600. The tempering holding time was set to 3, 6, 9, and 12 h at the tempering temperature of 500 °C, furnace-cooled, and the samples were recorded as QT3h, QT6h, QT9h, and QT12h.

Table 1 XRF analysis composition data of HHCCI (wt.%)

C	Cr	Mn	Mo	Si	S	P	Fe
4.07	35.22	0.61	1.96	0.41	0.009	0.019	Bal

2.2 Microstructure Observation

After rough grinding, fine grinding, and fine polishing, the sample was etched with aqua regia for 10 s, and the microstructure was observed by scanning electron microscope (SEM, Gemini 300 Zeiss). Image-Pro Plus was used to count the volume fraction of primary and eutectic carbide phases in the HHCCI after tempering on five SEM pictures with 200 × magnification and took the average value as the result. The volume fraction and equivalent diameter of secondary carbides were calculated by using 30,000 × SEM pictures, and the equivalent diameter of secondary carbides was calculated by the formula 1.

$$D = 2\sqrt{\frac{A}{\pi N}} \quad (\text{Eq 1})$$

where A is the total area of secondary carbides in a field of view, N is the total number of secondary carbides in a field of view. The average value was calculated using five photos randomly selected from each sample. Thin areas were obtained by pit instrument (Gaten 651) and ion thinning instrument (Leica EMRES 102), and transmission electron microscope samples were prepared. The types and crystallography of secondary carbides were investigated by JEOL-2100F transmission electron microscope (TEM).

2.3 X-ray Diffraction (XRD) Analysis

The samples were analyzed by XRD with an x-ray diffractometer (Bruker D8 ADVANCE, Germany). A Cu K α -ray source ($\lambda = 0.15418$ nm) with a voltage of 40 kV and a current of 30 mA was used, coupled with continuous scanning in the 2 θ range of 30-100° with a step size of 0.02° and a scanning speed of 1.5°/min.

2.4 Hardness Test

HBRV-187.5 Brauwell hardness tester was used to test the macrohardness with 1470 N load and 5 s residence time. The microhardness was tested using the MICROMET-5103 digital micro-hardness tester, the test load was 1.96 N, and the residence time was 10 s. In the microhardness and macrohardness test, 7 readings were randomly selected on the sample surface, and the average value was calculated after eliminated the maximum and minimum values.

3. Results and Discussions

3.1 Microstructure Evolution After Tempering at Different Temperatures

After heat treatment at different tempering temperatures, the SEM pictures of HHCCI are shown in Fig. 1. The microstructure after tempering consists of primary M₇C₃ carbides, eutectic M₇C₃ carbides, and matrix. The change in carbide volume fraction after tempering at different temperatures is shown in Fig. 2. After tempering, the volume fraction of the carbide phase does not change obviously with the increase in tempering temperature, primary carbides and eutectic carbides account for more than 40% of the field of view. From the microstructure image in Fig. 1, the morphology of primary carbides and eutectic carbides did not change significantly with the contin-

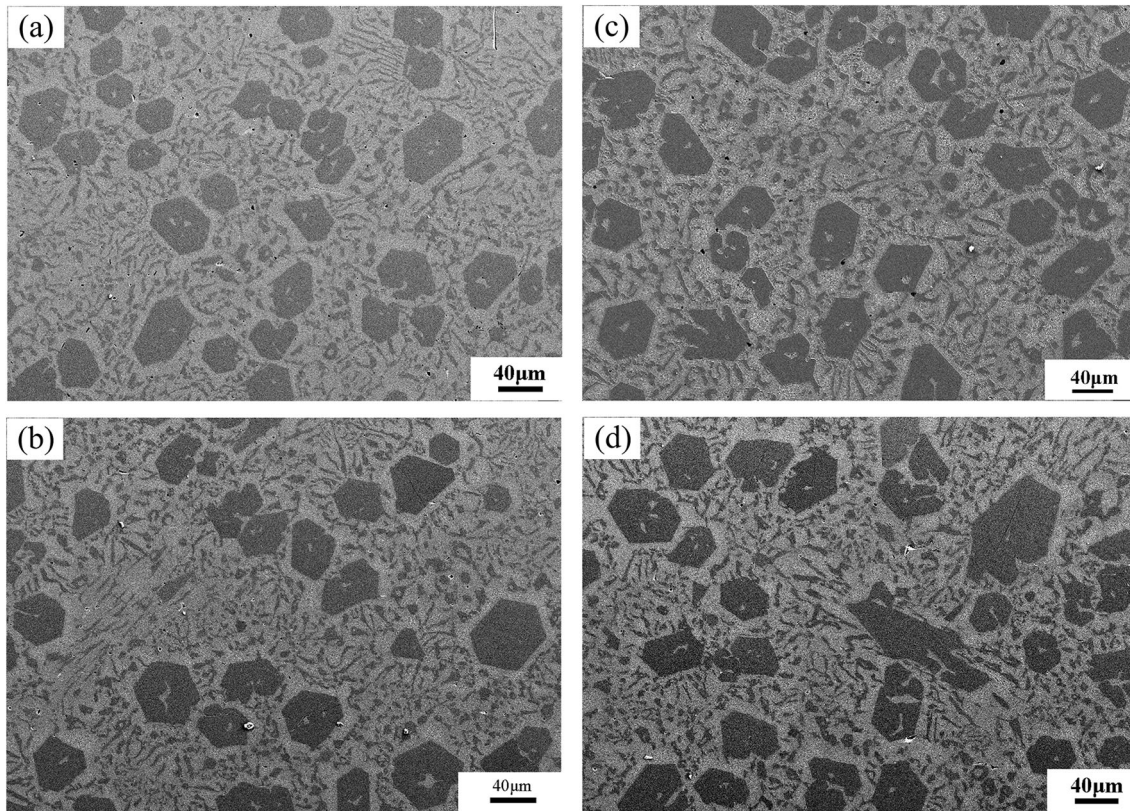


Fig. 1 SEM images of HHCCI after reheating to 1025 °C for 1 h then air-cooling quenching and tempering at different temperatures: (a) QT200, (b) QT400, (c) QT500, (d) QT600

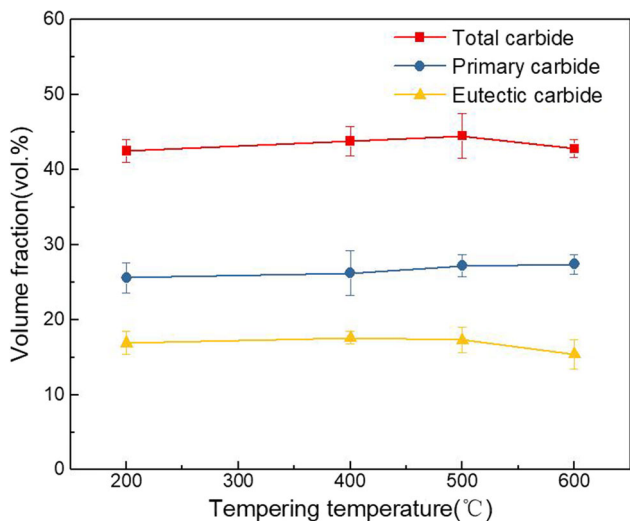


Fig. 2 Effect of tempering temperature on volume fraction of carbides in HHCCI after holding time for 3 h

uous increase of tempering temperature. This phenomenon shows that the main adjustment of tempering temperature is the matrix structure, which has little effect on the adjustment of primary carbides and eutectic carbides (Ref 17).

The high-magnification SEM observation of the matrix is shown in Fig. 3. The diffusion of C atoms mainly occurs in the matrix after tempering temperature at 200 °C, which can eliminate some residual internal stress and form tempered martensite (Ref 18). Due to the low tempering temperature and

the slow diffusion speed of Cr and C atoms, it is difficult for alloy elements to gather together to form new carbides during tempering. The secondary carbides precipitated by the quenching treatment grow up during tempering holding time. Due to the above reasons, the number of secondary carbides precipitated from the matrix structure tempered at 200 °C is less, and the particle size is larger. Combined with the SEM images, the volume fraction and equivalent diameter of secondary carbides in the matrix after tempering at different temperatures were statistically calculated by Image Pro Plus software, and the result is shown in Fig. 4. According to the statistical data, the volume fraction of secondary carbides in the matrix after tempering at 200 °C is about 33%, and the average equivalent diameter is about 160 nm.

When the tempering temperature rises to 400 °C, the diffusion of C and alloying elements in the martensitic matrix accelerates and begins to gather together to precipitate secondary carbides from the matrix (Ref 19). At the same time, secondary carbides are also precipitated from the retained austenite, which reduces the content of C and alloying elements, and reduces the stability of the austenite, resulting in a transformation of retained austenite to martensite. Figure 5 shows the XRD patterns of the samples at different tempering temperatures. The phase composition of the sample was determined by comparing the XRD spectrum of the sample with the standard spectrum. Austenite (52-0512), martensite (44-1290), M_7C_3 (05-0720), and $M_{23}C_6$ (78-1502) PDF cards were used in the experiment. The XRD results show that there is still some retained austenite in the matrix after tempering at 400 °C. As can be seen from Fig. 3(b), the secondary carbides in the matrix can be roughly divided into two regions. The

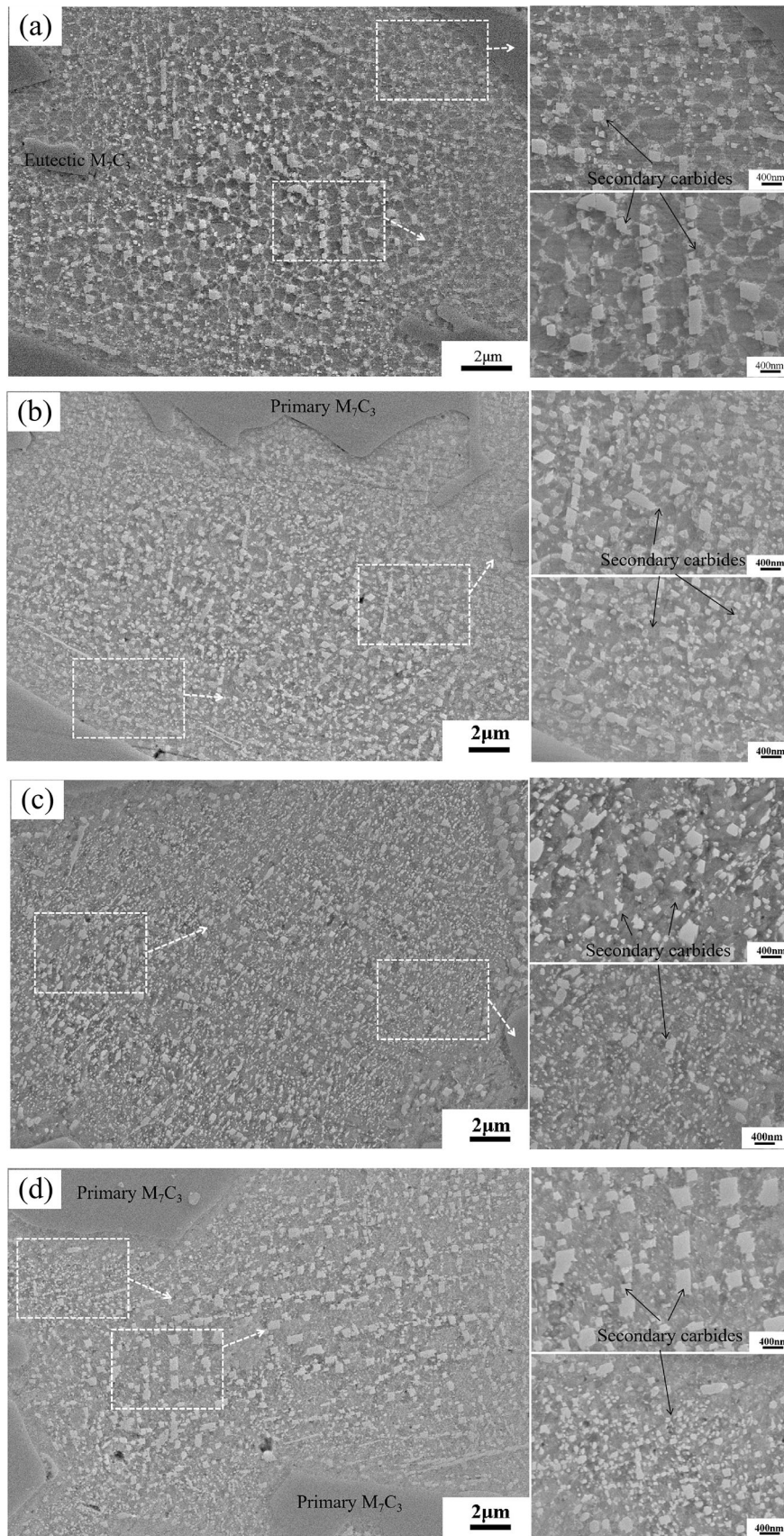
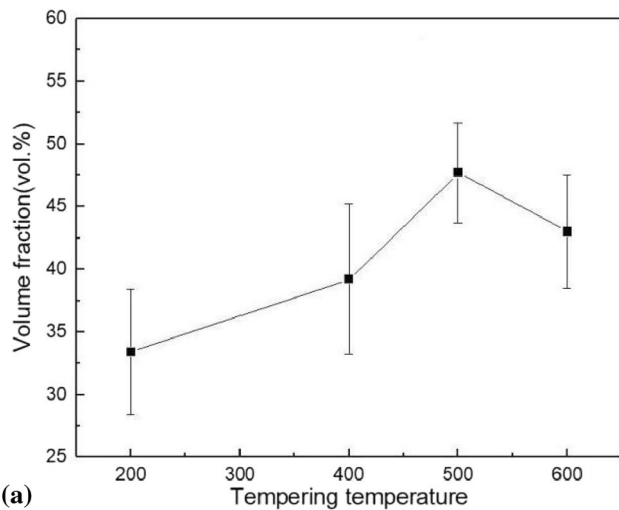
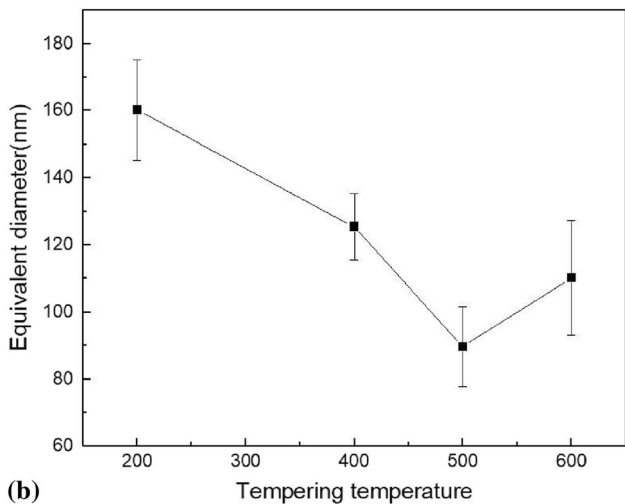


Fig. 3 High magnification SEM pictures of the matrix of HHCCI at different tempering temperatures for 3 h: (a) QT200, (b) QT400, (c) QT500, (d) QT600



(a)



(b)

Fig. 4 Effect of holding time for 3 h at different tempering temperature on volume fraction (a) and equivalent diameter (b) of secondary carbides in the matrix

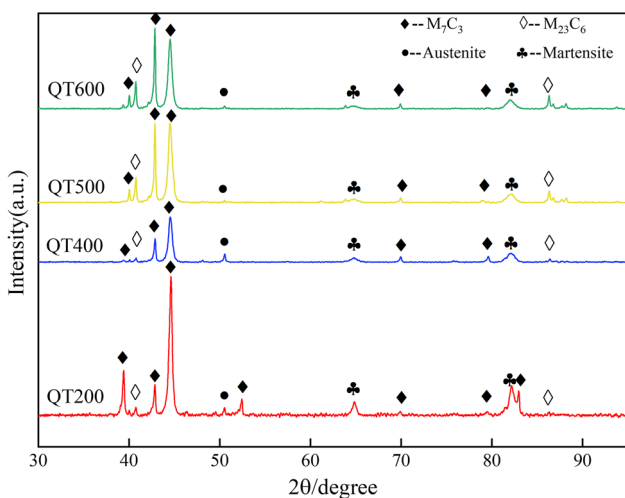


Fig. 5 XRD spectra of HHCCI at different tempering temperatures for 3 h

secondary carbides near the primary and eutectic carbides are fine and uniform. In the “central” region away from the primary and eutectic carbides, the precipitated secondary carbides are larger in size and agglomerate. This is because, during the solidification of molten iron, the primary and eutectic carbides take away some C and Cr atoms from the surrounding matrix during the growth process, so that the secondary carbides precipitated from the surrounding matrix during subsequent quenching and tempering, and the size is smaller than that of the central region. The “central” area, away from primary and eutectic carbides, has high C and Cr content. During the tempering process, more C and alloy elements can dissolve from the matrix structure and combine to form secondary carbides, which will grow up and agglomerate in the subsequent tempering holding process.

It can be seen from Fig. 3(c) that the carbides precipitated in the matrix further increase after tempering at 500 °C, and the secondary carbides are fine and uniformly distributed. When the tempering temperature is raised to 500 °C, the diffusion speed of C and alloy elements in martensite is further accelerated, resulting in easier to gather together to form secondary carbides. At this time, the changes in secondary carbides mainly have three aspects. On the one hand, the secondary carbides were precipitated and grow up during the tempering and holding process (Ref 20). On the other hand, the retained austenite loses stability during tempering, and the precipitated C atoms and Cr atoms interact to form secondary carbides (Ref 21). It can be seen from the XRD results in Fig. 5 that when the temperature reaches above 500 °C, the retained austenite was completely decomposed and transformed into martensite and secondary carbides after quenching. Thirdly, as the tempering temperature increases, the diffusion rate of each atom is accelerated, and the secondary carbides are precipitated while the martensite is decomposed (Ref 22). Due to the above factors, more secondary carbides precipitated in the matrix, and the average volume fraction of secondary carbides in the matrix is about 47%. As the tempering temperature increases to 600 °C, more and more martensite decomposes and secondary carbides are precipitated. At the same time, with the increase of tempering temperature, carbides accumulate, grow and coarsen, and gradually change from granular to thin strips (Ref 23). Combined with Fig. 3(d) and 4(b), it can conclude that the aggregation and growth of secondary carbides decrease the volume fraction and increase the average particle size of secondary carbides, which is 89 nm at 500 °C and 110 nm at 600 °C.

In order to determine the type and crystal structure of the secondary carbides precipitated after tempering, the samples were observed by TEM after ion thinning. From the TEM image in Fig. 6, the secondary carbides precipitated in the matrix after tempering are $M_{23}C_6$. The $M_{23}C_6$ precipitated at 200 °C is rectangular, with larger particles and less precipitation. With the increase of the tempering temperature, the precipitated $M_{23}C_6$ becomes finer, the edge gradually becomes round, and the number increases continuously. When the tempering temperature is 500 °C, the secondary carbide particles are fine, the number is the largest, and the distribution is dispersed. According to the literature (Ref 24, 25), there are many different orientations between martensitic matrix and $M_{23}C_6$ from, such as $(111)M_{23}C_6 \parallel (111)\alpha'-Fe$ and $[011]M_{23}C_6 \parallel [011]\alpha'-Fe$ or $(111)M_{23}C_6 \parallel (011)\alpha'-Fe$ and $[011]M_{23}C_6 \parallel [111]\alpha'-Fe$. Figure 7 shows a high-resolution image of the martensite and $M_{23}C_6$ in the QT500 sample. It can be seen

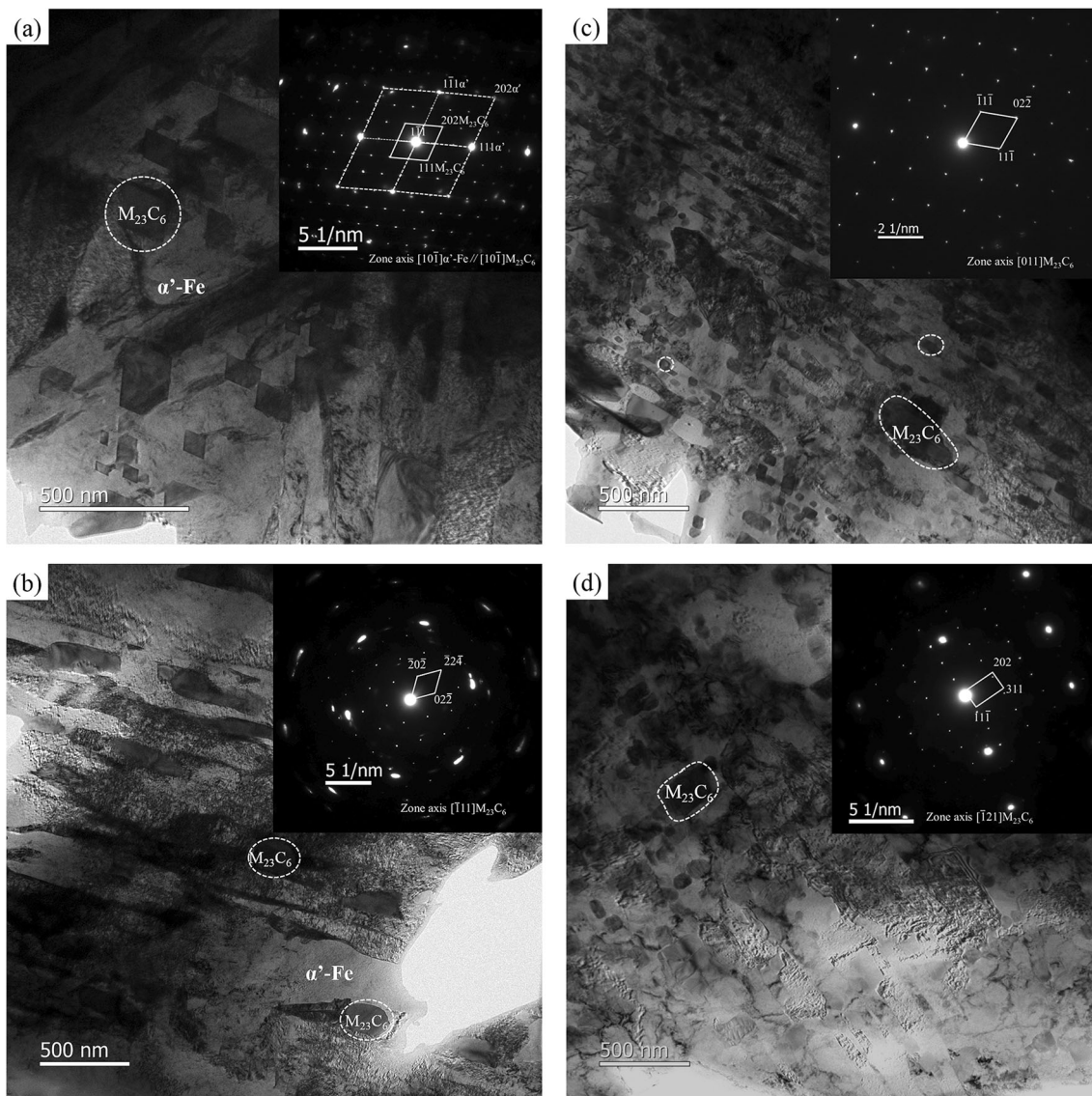


Fig. 6 TEM images and the corresponding SADPS of HHCCI after tempering at different temperatures for 3 h: (a) QT200, (b) QT400, (c) QT500, (d) QT600

that the crystal plane spacing of $(101)\alpha'$ -Fe and $(303)M_{23}C_6$ is similar, and the atomic arrangement direction is approximately parallel, indicating that the interface bonding relationship between martensite and $M_{23}C_6$ is good. The microhardness of martensite is about 300-900 HV, and the microhardness of $M_{23}C_6$ is about 1000-1150 HV (Ref 26), so the fine dispersed secondary carbides precipitated after tempering can play a role in dispersion strengthening and improve the hardness of the material.

3.2 Effect of Tempering Temperature on Hardness

The hardness change of HHCCI after tempering at different temperatures is shown in Fig. 8. During the tempering and holding stage at different temperatures, the diffusion speed of C and alloy elements increases with the increase of tempering temperature. The secondary quenching of retained austenite, the transformation and decomposition of quenched martensite, and the growth of precipitated carbides have a direct impact on the microhardness and macrohardness of the materials. The

favorable microstructure transformation of microhardness is divided into two aspects. In the first aspect, a part of retained austenite will undergo secondary quenching and transform into martensite, the hardness of martensite is higher than that of austenite. In the second aspect, the continuous precipitation and uniform distribution of secondary carbides on the matrix are also beneficial to improve the hardness of the matrix. And there are two aspects of adverse microstructure change. On the one hand, the quenched martensite decomposes during the tempering process, reducing the content of C and alloying elements, and resulting in softening of the matrix microstructure. On the other hand, with the increase of temperature, the tendency of coarsening and aggregation of secondary carbides becomes more obvious (Ref 27). The combination of the above favorable and unfavorable factors makes the hardness of the material vary depending on which factor dominates.

When tempered at 200 °C, the internal stress of the matrix structure is eliminated. Due to the low tempering temperature, the secondary carbides precipitated before quenching mainly grow and segregate, which have no obvious effect on the

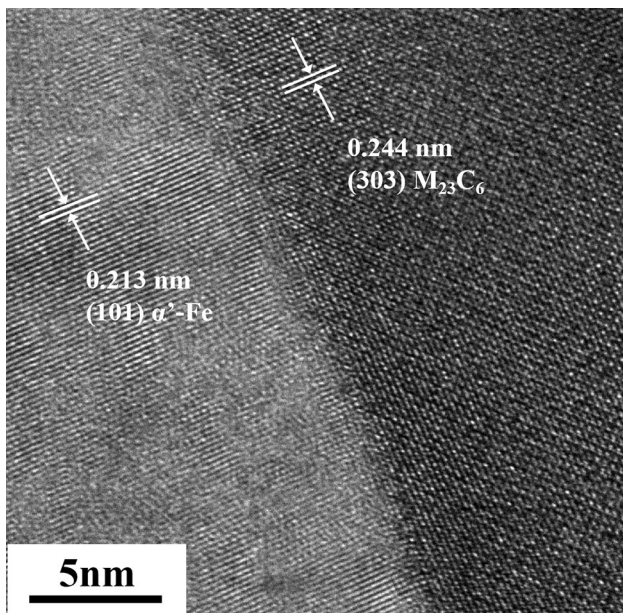


Fig. 7 HRTEM images of matrix and secondary carbides in the sample after tempering at 500 °C for 3 h

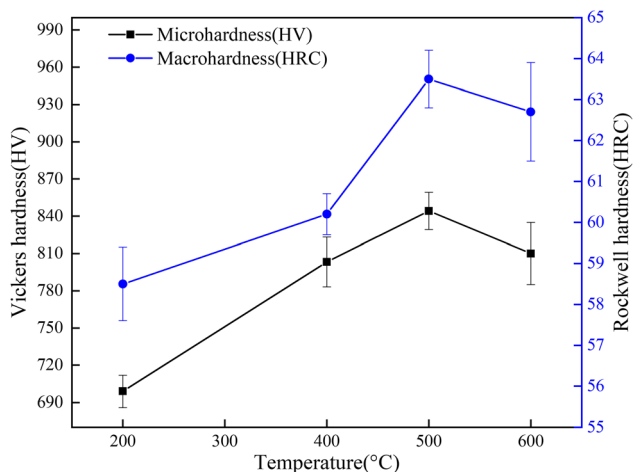


Fig. 8 Effect of holding time for 3 h at different tempering temperatures on the hardness of HHCCI

microstructure and property of the matrix. When the tempering temperature is increased to 400–500 °C, the retained austenite is transformed into martensite, and the precipitation of fine and dispersed secondary carbides compensates for the tempering softening of martensite, which makes the microhardness and macrohardness increase obviously. As the tempering temperature further increases, the decomposition of martensite and the growth of pre-precipitated secondary carbides begin to dominate, which will lead to a decrease in hardness.

3.3 Microstructure Evolution After Tempering at Different Holding Times

SEM images of HHCCI tempered at 500 °C for different holding times are shown in Fig. 9. Combined with the XRD results in Fig. 10, the change in the tempering holding time

does not change the type of carbide in HHCCI. The microstructure of HHCCI consists of primary M_7C_3 carbides, eutectic M_7C_3 carbides, martensite, and retained austenite. With the prolongation of the tempering holding time, the morphology of primary M_7C_3 carbides changes little. The eutectic carbides also continue to aggregate and grow. From the statistical volume fraction results of each phase after tempering (as shown in Fig. 11), the content of primary carbides did not change much, and the volume fraction of eutectic carbides gradually decreased from 17.3 to 14.5%. It shows that with the prolongation of the tempering holding time, the eutectic carbides begin to grow and agglomerate, and at the same time, part of the eutectic carbides re-decompose and dissolve into the matrix.

The high-magnification SEM observation of the matrix is shown in Fig. 12. It can be seen from the discussion in the previous section that during the heat treatment process of tempering at 500 °C for 3 h and furnace cooling, the diffusion rate of C and Cr atoms is faster, a part of retained austenite will undergo secondary quenching and transform into tempered martensite and partially decomposes, and the secondary carbides (mainly $M_{23}C_6$) precipitate and grow, these make the secondary carbides precipitated after tempering at 500 °C for 3 h finer and more uniform, playing the role of secondary hardening and dispersion strengthening. The volume fraction and equivalent diameter of secondary carbides in the matrix after tempering at different holding times are obtained by using Image Pro Plus software, as shown in Fig. 13. When the holding time increases from 3 to 6 h, the precipitated secondary carbides increase and grow up, the volume fraction of secondary carbides in the matrix changes from 47 to 54%, and the average equivalent diameter increases from 89 to 130 nm. Especially in the “central” region of the matrix away from primary and eutectic carbides, the diameter of secondary carbides can reach 300–400 nm. With the further extension of holding time, the equivalent diameter of carbide increases, but the volume fraction in the matrix decreases. After tempering for 12 h, the equivalent diameter of secondary carbides increases to 240 nm and the volume fraction decreases to 39%.

With the extension of holding time, the retained austenite almost transforms into martensite. At the same time, martensite decomposes continuously during tempering. Strong carbide formers (Cr and Mo, etc.) in the quenched martensitic matrix continue to bond with C atoms at higher temperatures. While the secondary carbides are precipitated continuously, the secondary carbides of the first precipitation also aggregate and grow. As shown in Fig. 14(a), the quenched martensite transforms into a mixture of α -Fe and secondary carbides of about a few nm after decarburization. These secondary carbides can act as nucleation sites to combine C and alloying elements and grow (Fig. 14b). With the further increase in the holding time, more alloying elements and C elements in the martensite matrix will be desolubilized. Due to a large number of precipitated secondary carbides, the precipitated alloying elements are more inclined to combine with the precipitated carbides rather than continue to precipitate new carbides, resulting in the continuous growth of the carbides, and the growth of the particles from initially smooth particles into long blocks. The adjacent secondary carbides with similar orientations tend to grow up and combine together at a higher temperature. This abnormal length means that several square particles combine to grow large particles, which are arranged side by side in different directions, resulting in a net distribution

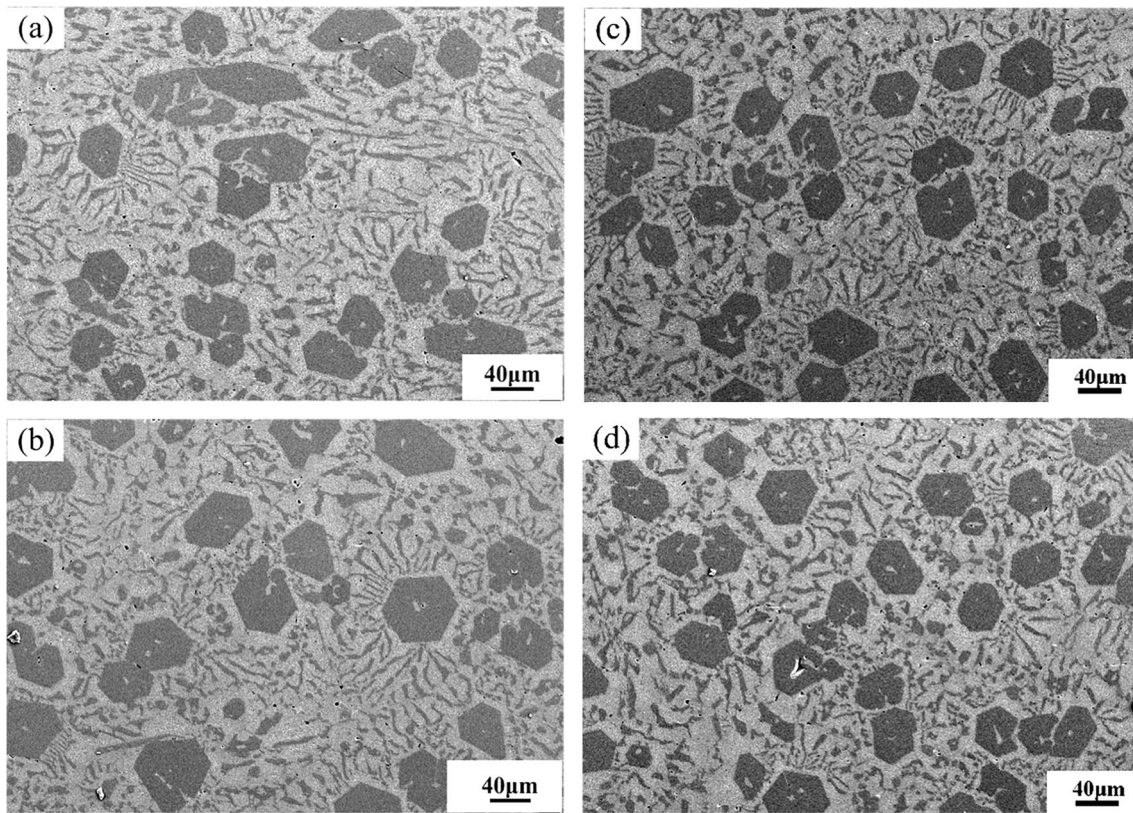


Fig. 9 SEM pictures of HHCCI after 1025 °C for 1 h then air-cooling quenching and tempering at 500 °C for different holding times: (a) QT3h, (b) QT6h, (c) QT9h, (d) QT12h

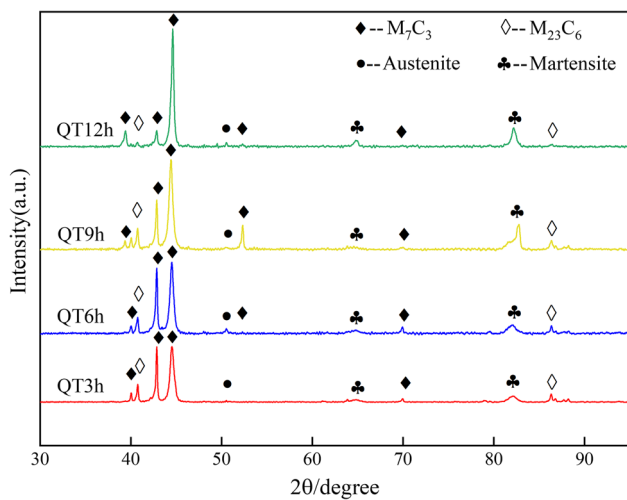


Fig. 10 XRD spectra of HHCCI with different tempering times at 500 °C

of some secondary carbides in the matrix. As shown in Fig. 12(b-d), with the increase of holding time, the tendency of long carbides to form a network in the matrix is more obvious. After the tempering holding time reached 12 h, the carbides precipitated in the matrix grew near the primary and eutectic carbides, and the particles in the “center” region of the matrix

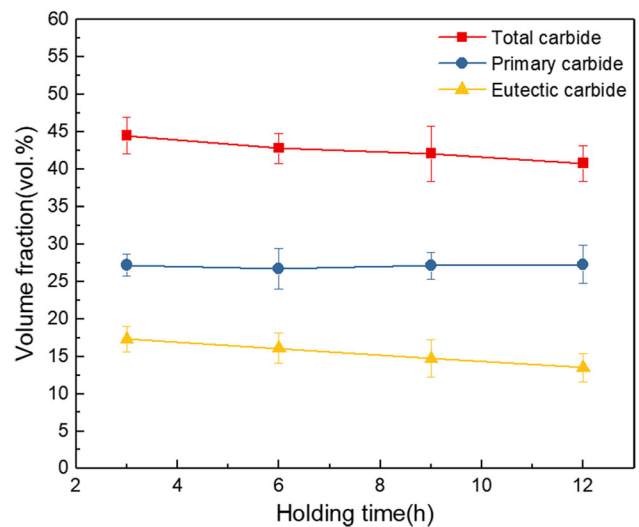


Fig. 11 Effect of tempering holding times on carbide volume fraction of HHCCI at tempering temperature of 500 °C

even grew to an equivalent diameter of 1 μm or larger, and more secondary carbides gather together. It can be seen from the micrograph of Fig. 12(d) that part of the large particle size and long carbides have fallen off from the matrix under the same etching conditions. The SEM and TEM images in Fig. 15 show the abnormal aggregation of $M_{23}C_6$ carbides observed

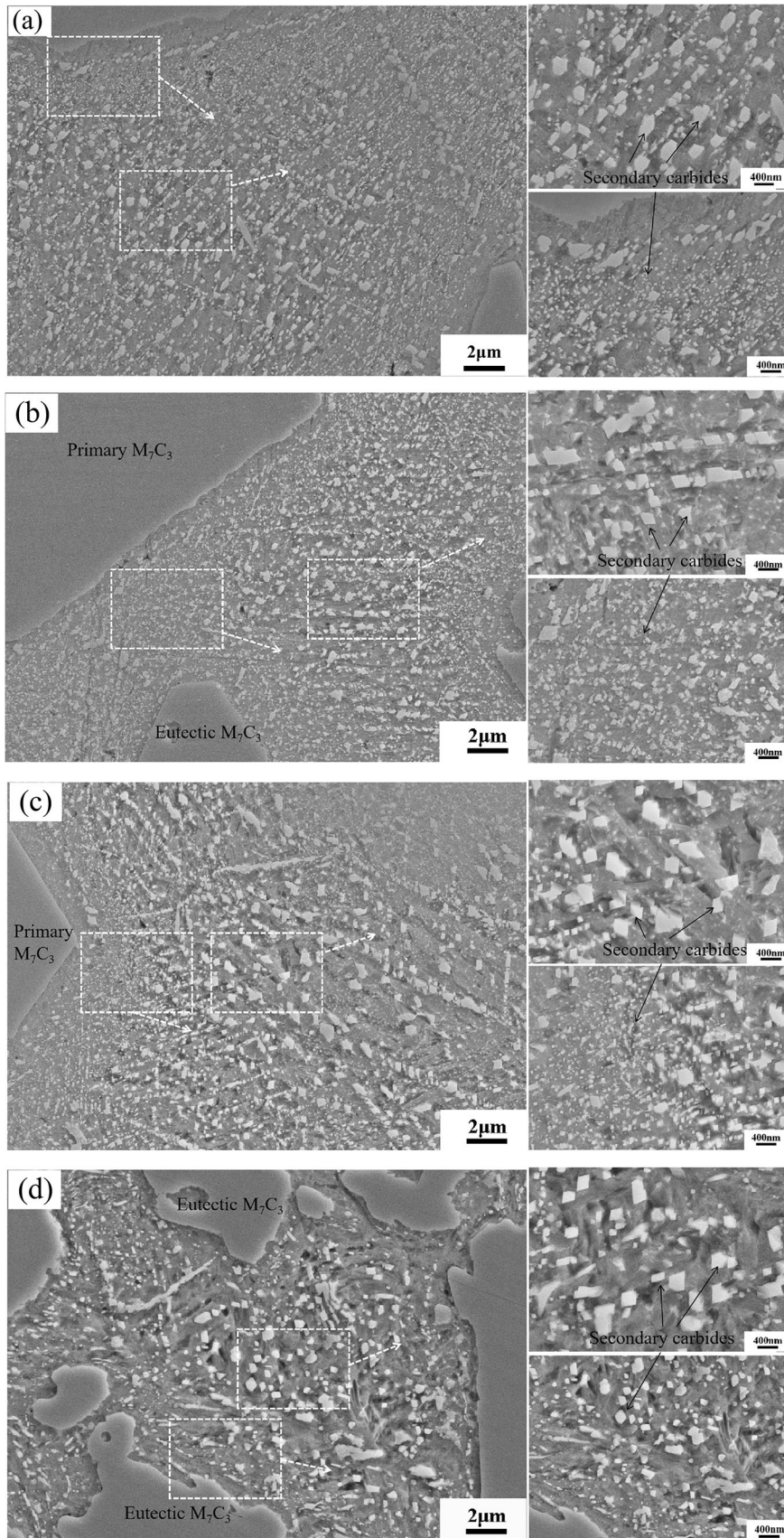


Fig. 12 High magnification SEM pictures of the matrix of HHCCI after tempering at 500 °C for different holding times: (a) QT3h, (b) QT6h, (c) QT9h, (d) QT12h

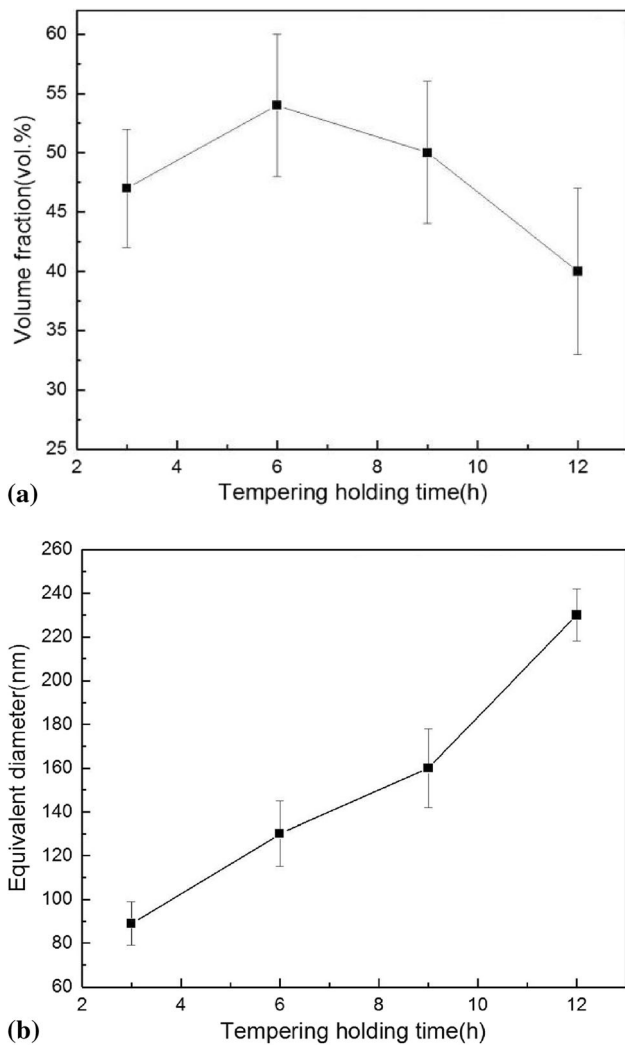


Fig. 13 Volume fraction (a) and equivalent diameter (b) of secondary carbides in matrix after tempering at 500 °C for different holding times

after tempering and holding at 500 °C for 9 and 12 h. A certain number of $M_{23}C_6$ with similar orientation aggregate and grow into a long strip-shaped secondary carbide combination, and its length can reach several microns to more than 10 microns. The coarsening and abnormal distribution of secondary carbides greatly reduce their support for the matrix, which may adversely affect the properties of the material.

3.4 Effect of Tempering Holding Time on Hardness

The microhardness and macrohardness of HHCCI after tempering at 500 °C with different holding times are shown in Fig. 16. After tempering at 500 °C for 3 h, the retained austenite transforms into martensite by secondary quenching, and is dominated by fine and dispersed secondary carbides. With the increase of tempering holding time, the dispersion strengthening and secondary hardening of precipitated carbides become more obvious, which counteracts the negative effect of

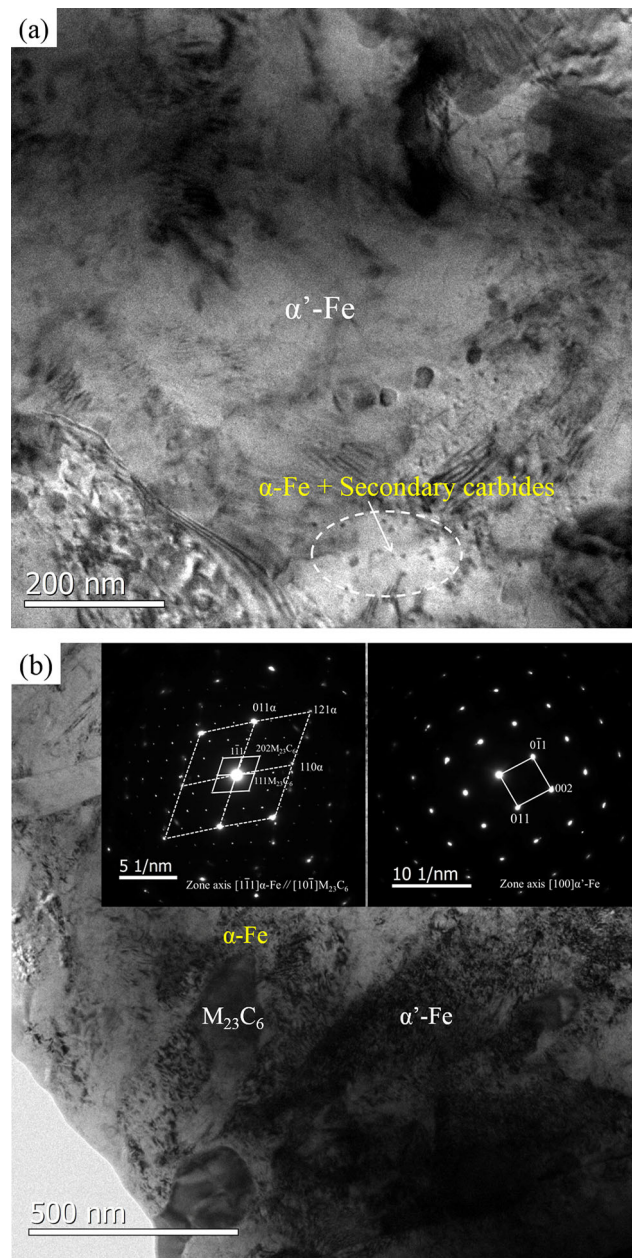


Fig. 14 Decomposition of martensite during tempering: (a) TEM picture of matrix after tempering at 500 °C for 6 h, (b) TEM pictures of $M_{23}C_6$ and ferrite in the matrix and corresponding SADPs after tempering at 500 °C for 9 h

martensite decomposition. After tempering for 6 h, the volume fraction of secondary carbides in the matrix is the largest (as shown in Fig. 13), and the distribution is dispersed with a smaller particle size, which increases the microhardness of the matrix. As a result, the macrohardness of HHCCI increases from 63.5 to 66.0 HRC, reaching the peak value of hardness. With the further increase of holding time, the trend of coarsening growth and abnormal aggregation of secondary carbides becomes more obvious. At the same time, the

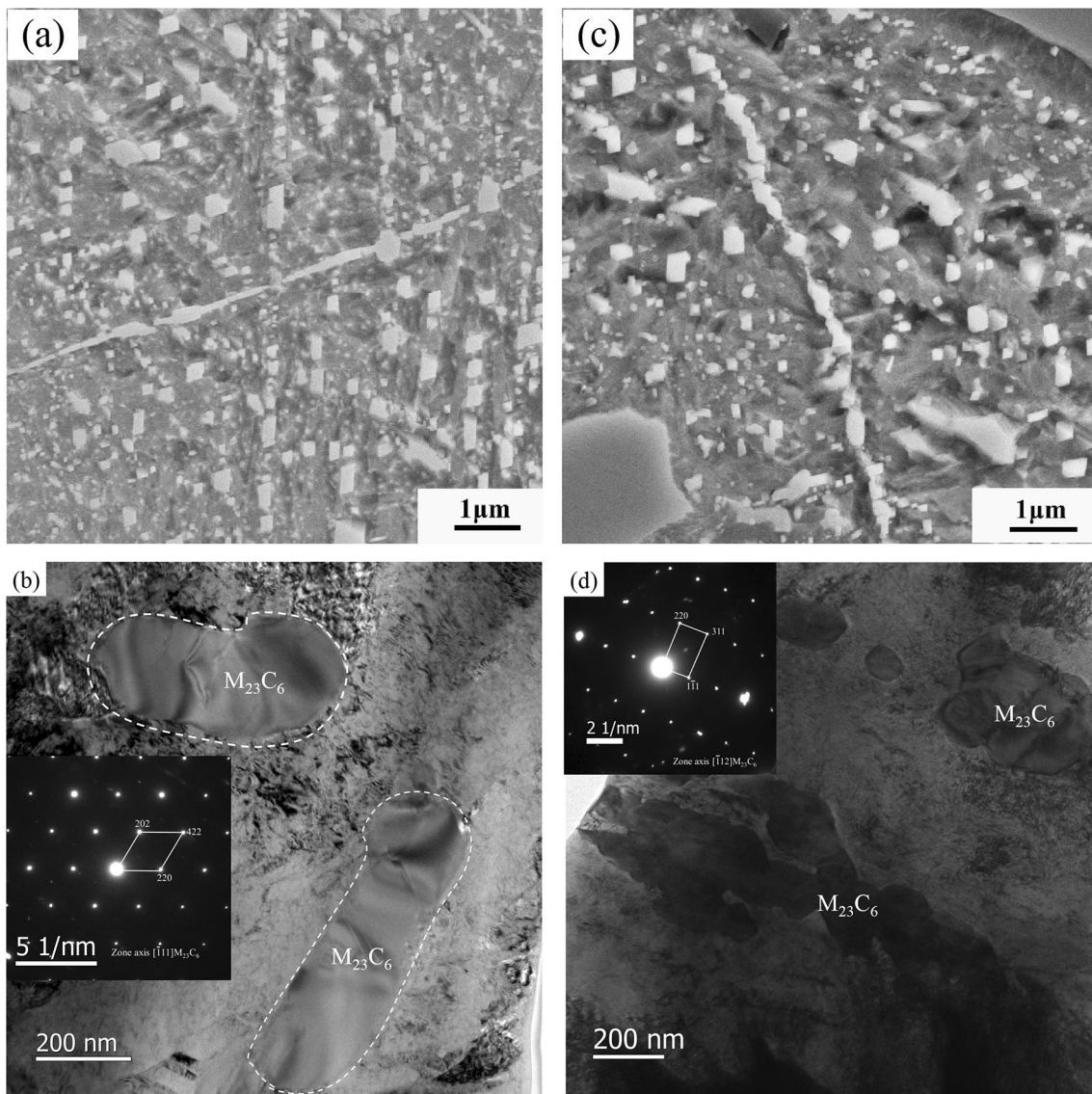


Fig. 15 SEM and TEM pictures of secondary carbide $M_{23}C_6$ in matrix after tempering at 500 °C for different times: (a), (b) QT9h; (c), (d) QT12h

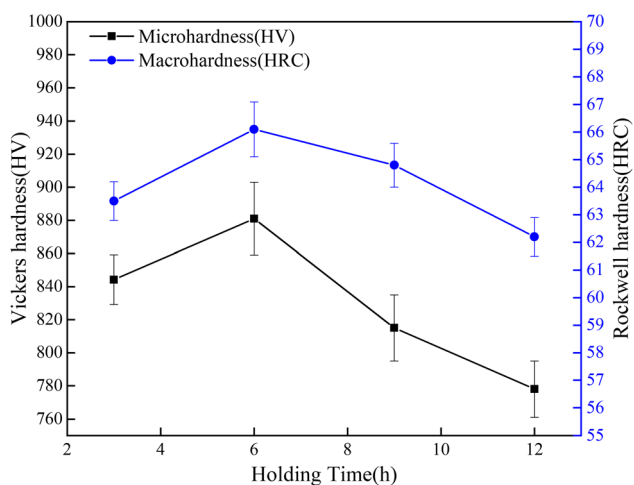


Fig. 16 Effect of tempering holding times on the hardness of HHCCI at tempering temperature of 500 °C

tempering softening effect of martensite decomposition is gradually enhanced, resulting in a sharp decline in the hardness of HHCCI. After tempering for 9 and 12 h, respectively, the microhardness of the matrix and the macrohardness of HHCCI are significantly lower than that of tempering for 6 h.

4. Conclusions

The present work investigates the effect of the tempering process on the microstructure evolution and hardness of 35 wt.%Cr—4 wt.%C hypereutectic high chromium cast iron. The main results are summarized as follows:

- (1) The tempered microstructure of hypereutectic high chromium cast iron consists of primary M_7C_3 carbides, eutectic M_7C_3 carbides, martensitic, and retained austenite. With the increase of tempering temperature, the changes of primary carbides and eutectic carbides are not obvious,

and the precipitation of secondary carbides in the matrix increases at first and then decreases. With the prolongation of the tempering holding time, the eutectic carbides partially decompose into the matrix, and the secondary carbides continue to precipitate and grow.

- (2) The main sources of secondary carbides precipitation in the matrix during the tempering process are the destabilization of retained austenite and the decomposition of martensite, and the main type is $M_{23}C_6$. The secondary carbides near the primary and eutectic carbides are finer and more uniform. The secondary carbides precipitated in the “central” region far from the primary and eutectic carbides are larger in size and tend to agglomerate.
- (3) After tempering at 200–600 °C for 3 h, the hardness of HHCCI increases with the increase of tempering temperature. The highest hardness is 63.5 HRC at 500 °C. Continuously increasing the tempering temperature will lead to a decrease in hardness.
- (4) After tempering at 500 °C for 3–12 h, the hardness of HHCCI increases with the extension of the tempering holding time, and the hardness reaches the highest value of 66.0 HRC when the tempering holding time is 6 h. Continuously prolonging the holding time will result in a decrease in hardness.

Acknowledgment

The authors would like to thank the financial support for this work from National Natural Science Foundation of China (52075010), and Hebei Science and Technology Major Project (22281005Z).

References

1. J. Wang, X. Ji, H. Fan, H.S. Yang, H.H. Liu, and B.L. Shen, Effects of High Temperature and Cryogenic Treatment on the Microstructure and Abrasion Resistance of a High Chromium Cast Iron, *J. Mater. Process. Technol.*, 2009, **209**(7), p 3236–3240
2. Q.H. Cen, H.B. Zhang, and H.G. Fu, Effect of Heat Treatment on Structure and Wear Resistance of High Chromium Cast Steel Containing Boron, *J. Iron Steel Res. Int.*, 2014, **21**(5), p 532–538
3. X.H. Zhi, J.D. Xing, H.G. Fu, and M. Yi, Effect of Titanium on the As-Cast Microstructure of Hypereutectic High Chromium Cast Iron, *Mater. Charact.*, 2008, **59**(9), p 1221–1226
4. N. Barnes, S. Clark, S. Seetharaman, and P.F. Mendez, Growth Mechanism of Primary Needles During the Solidification of Chromium Carbide Overlays, *Acta Mater.*, 2018, **151**, p 356–365
5. Z.Y. Zhao, R.B. Song, Y.C. Zhang, P. Yu, and Y. Pei, Co-orientation Relationship between Secondary Carbides and Adjacent Ferrite after Quenching and Tempering in High Chromium Cast Iron, *Vacuum*, 2021, **184**, p 109911
6. Y.C. Li, P. Li, K. Wang, H.Z. Li, M.Y. Gong, and W.P. Tong, Microstructure and Mechanical Properties of a Mo Alloyed High Chromium Cast Iron After Different Heat Treatments, *Vacuum*, 2018, **156**, p 59–67
7. M.A. Guitart, S. Suárez, O. Prat, M. Duarte Guigou, V. Gari, G. Pereira, and F. Mücklich, High Chromium Cast Irons: Destabilized-Subcritical Secondary Carbide Precipitation and Its Effect on Hardness and Wear Properties, *J. Mater. Eng. Perform.*, 2018, **27**(8), p 3877–3885
8. A.S. Jain, H.W. Chang, X.H. Tang, B. Hinckley, and M.X. Zhang, Refinement of Primary Carbides in Hypereutectic High-Chromium Cast Irons: a review, *J. Mater. Sci.*, 2021, **56**(2), p 999–1038
9. L. Lu, H. Soda, and A. Mclean, Microstructure and Mechanical Properties of Fe–Cr–C Eutectic Composites, *Mater. Sci. Eng. A.*, 2003, **347**(1), p 214–222
10. Q. Guo, H.G. Fu, X.Y. Guo, Z.G. Xing, and J. Lin, Microstructure and Properties of Modified As-Cast Hypereutectic High Chromium Cast Iron, *Materialwiss. Werkstofftech.*, 2022, **2**, p 53
11. S. Zhou, Y. Shen, H. Zhang, and D. Chen, Heat Treatment Effect on Microstructure, Hardness and Wear Resistance of Cr26 White Cast Iron, *Chin. J. Mech. Eng.*, 2015, **28**(1), p 140–147
12. S. Inthidech, K. Boonmak, P. Sricharoenchai, N. Sasaguri, and Y. Matsubara, Effect of Repeated Tempering on Hardness and Retained Austenite of High Chromium Cast Iron Containing Molybdenum, *Mater. Trans.*, 2010, **51**(7), p 1264–1271
13. G.P. Alejandro, A.L. Juan, Á.A. Florentino, and G.D. Ana, Improvement of Impact Toughness and Abrasion Resistance of a 3C–25Cr–0.5Mo Alloy Using a Design of Experiment Statistical Technique: Microstructural Correlations after Heat Treatments, *Metals*, 2021, **11**(4), p 595
14. A.F. Farah, O.R. Crnkovic, and L.C.F. Canale, Heat Treatment in High Cr White Cast Iron Nb Alloy, *J. Mater. Eng. Perform.*, 2001, **10**(1), p 42–45
15. K.K. Singh, R.S. Verma, and G.M.D. Murty, Optimizing Wear Resistance and Impact Toughness in High Chromium Iron Mo-Ni Alloy, *J. Mater. Eng. Perform.*, 2009, **18**(4), p 438–440
16. Z.Y. Chen, Q. Guo, H.G. Fu, and X.H. Zhi, Effect of Heat Treatment on Microstructure and Properties of Modified Hypereutectic High Chromium Cast Iron, *Mater. Test.*, 2022, **64**(1), p 33–54
17. A. Wiengmoon, T. Chairuangri, A. Brown, R. Brydson, D.V. Edmonds, and J.T.H. Pearce, Microstructural and Crystallographical Study of Carbides in 30wt.%Cr Cast Irons, *Acta Mater.*, 2005, **53**(15), p 4143–4154
18. J.J. Hao, J. Chen, and P.D. Han, Solid Phase Decarburization Kinetics of High-Carbon Ferrochrome Powders in the Microwave Field, *Steel Res. Int.*, 2014, **85**(3), p 461–465
19. K. Weber, D. Regener, H. Mehner, and M. Menzel, Characterization of the Microstructure of High-Chromium Cast Irons Using Mossbauer Spectroscopy, *Mater. Charact.*, 2001, **46**(5), p 399–406
20. G.M. Agustina, S. Anna, S. Sebastián, B. Dominik, G.M. Duarte, and M. Frank, Secondary Carbides in High Chromium Cast Irons: An Alternative Approach to Their Morphological and Spatial Distribution Characterization, *Mater. Charact.*, 2018, **144**, p 621–630
21. G. Powell and G. Laird, Structure, Nucleation, Growth and Morphology of Secondary Carbides in High Chromium and Cr-Ni White Cast Irons, *J. Mater. Sci.*, 1992, **27**(1), p 29–35
22. A. Wiengmoon, J.T.H. Pearce, S. Nusen, and T. Chairuangri, Electron Microscopy Study of Carbides Precipitated During Destabilization and Tempering Heat Treatments of 25 wt.%Cr-07 wt.%Mo High Chromium Cast Irons, *Micron*, 2021, **143**, p 103025
23. J. Guo, L. Liu, Y. Feng, S. Liu, X. Ren, and Q. Yang, Crystallographic Characterizations of Eutectic and Secondary Carbides in a Fe-12Cr-2.5Mo-1.5W-3V-1.25C Alloy, *Met. Mater. Int.*, 2017, **23**(2), p 313–319
24. C.M. Lin, H.H. Lai, J.C. Kuo, and W. Wu, Effect of Carbon Content on Solidification Behaviors and Morphological Characteristics of the Constituent Phases in Cr-Fe-C Alloys, *Mater. Charact.*, 2011, **62**(12), p 1124–1133
25. W. Yong, Y.L. Mei, B. Han, H. Tao, and Y.C. Yi, Influence of Secondary Carbides Precipitation and Transformation on the Secondary Hardening of Laser Melted High Chromium Steel, *J. Mater. Sci.*, 2010, **45**(13), p 3442–3447
26. S. Imurai, C. Thanachayanont, J.T.H. Pearce, K. Tsuda, and T. Chairuangri, Effects of Mo on Microstructure of As-Cast 28 wt.%Cr-2.6 wt.%C-(0-10) wt.%Mo Irons, *Mater. Charact.*, 2014, **90**, p 99–112
27. H.G. Fu, Effect of Tempering on The Structure and Property of Rich Chromium Cast Iron, *Heat Treat. Met.*, 1994, **12**, p 7–9

Publisher's Note Springer Nature remains neutral with regard to jurisdictional claims in published maps and institutional affiliations.

Springer Nature or its licensor (e.g. a society or other partner) holds exclusive rights to this article under a publishing agreement with the author(s) or other rightsholder(s); author self-archiving of the accepted manuscript version of this article is solely governed by the terms of such publishing agreement and applicable law.